Design and construction of a cascading pressure reactor prototype for solar-thermochemical hydrogen production

Cite as: AIP Conference Proceedings **1734**, 120001 (2016); https://doi.org/10.1063/1.4949203
Published Online: 31 May 2016

Ivan Ermanoski, Johannes Grobbel, Abhishek Singh, Justin Lapp, Stefan Brendelberger, Martin Roeb, Christian Sattler, Josh Whaley, Anthony McDaniel, and Nathan P. Siegel

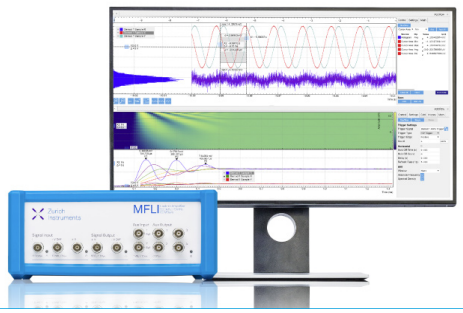

Design and Construction of a Cascading Pressure Reactor Prototype for Solar-Thermochemical Hydrogen Production

Ivan Ermanoski[1, a)], Johannes Grobbel[2], Abhishek Singh[3], Justin Lapp[3], Stefan Brendelberger[3], Martin Roeb[3], Christian Sattler[3], Josh Whaley[4], Anthony McDaniel[4], and Nathan P. Siegel[5]

[1]*Sandia National Laboratories, PO Box 5800, MS 1415, Albuquerque, NM 87123, USA*
[2]*German Aerospace Center, Professor-Rehm-Straße 1, 52428 Jülich, Germany*
[3]*German Aerospace Center, Linder Höhe,51147,Köln,Germany*
[4]*Sandia National Laboratories, Livermore, CA 94551, USA*
[5]*Mechanical Engineering Department, Bucknell University, Lewisburg, PA, 17837, USA*

[a)]Corresponding author: iermano@sandia.gov

Abstract. Recent work regarding the efficiency maximization for solar thermochemical fuel production in two step cycles has led to the design of a new type of reactor—the cascading pressure reactor—in which the thermal reduction step of the cycle is completed in multiple stages, at successively lower pressures. This approach enables lower thermal reduction pressures than in single-staged reactors, and decreases required pump work, leading to increased solar to fuel efficiencies. Here we report on the design and construction of a prototype cascading pressure reactor and testing of some of the key components. We especially focus on the technical challenges particular to the design, and their solutions.

INTRODUCTION

Two-step thermochemical cycles are a theoretically highly efficient and conceptually simple approach for solar fuel production. In the first step—thermal reduction—a reactive material (oxide) is partially or fully reduced at a high temperature. In the second step—fuel production—the reduced oxide is exposed to steam or CO_2 at a lower temperature, to produce H_2 or CO. Efficient two-step solar-thermochemical fuel production requires vacuum pumping or inert gas sweeping to lower the oxygen pressure in the thermal reduction step. Pumping is hampered by large oxygen volumetric flows, whereas sweeping is energy-intensive, requiring heat recovery at a high temperature, and a dedicated inert gas purification plant.[1-7]

A novel pumping approach— using a cascade of chambers at successively lower pressures—has been predicted to lead to over an order of magnitude pressure decrease compared to a single-chambered design.[8] To demonstrate the cascading reactor concept, as well as the whole cycle of a particle-based continuous H_2 production, with all the key components (receiver-reactors, water splitting, and particle lift) at realistic process temperatures and pressures, we have undertaken the design of a prototype device. This device will include two thermal reduction (TR) chambers, targeting ~100Pa and ~30Pa, while maintaining identical volumetric pumping speeds in both. The prototype is intended to be powered by a custom-built solar simulator, delivering a total of 3kW at the reactor apertures. The nominal project target is the production of 3stdl of H_2 in 8h of continuous operation, but based on the anticipated efficiency and input power, described below, a considerably higher output is expected. The design is compatible with any oxide in particle form, though initially intended to operate with CeO_2.

SolarPACES 2015
AIP Conf. Proc. 1734, 120001-1–120001-8; doi: 10.1063/1.4949203
Published by AIP Publishing. 978-0-7354-1386-3/$30.00

PROTOTYPE DESIGN ELEMENTS AND CHARACTERISTICS

Overview: Efficiency Model and Reactor Design

An anticipated prototype efficiency calculation, shown in FIGURE 1, comprehensively accounts for the heat equivalents of all energy inputs, and is described in detail in [9, 10]. Briefly, the reactor efficiency is the ratio of the H_2 output heat equivalent, and the sum of all required heat and heat equivalents of mechanical work. In addition to the energy inputs described in [9, 10], and considering the relatively small physical size of the prototype, a heat loss factor of 25% was included in the efficiency calculations. Furthermore, owing to the prototype design characteristics, all solid and gas heat recovery efficiencies were assumed to be zero. This is not strictly accurate, because some heating of the incoming steam will be accomplished by the hot reduced oxide and the heat of reoxidation reaction. Because the steam heating input is a small fraction of the total heat requirement, the approximation effect on efficiency is negligible. Importantly, the latter is true *only* when the steam and oxide flows in the water splitting (WS) step are countercurrent, as described in [9, 10].

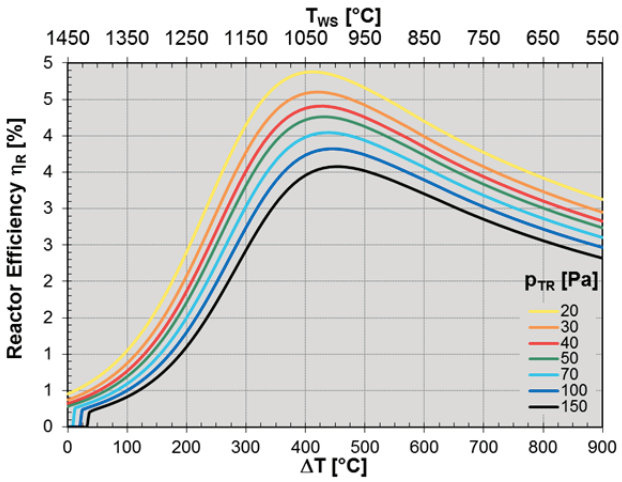

FIGURE 1. Calculated prototype reactor efficiency as function of ΔT (or T_{WS}), using ceria as the reactive oxide and operating at a TR temperature T_{TR}=1450°C, and several TR pressures $p_{TR,}$ corresponding to anticipated prototype conditions.

Based on the calculated efficiency and input power, the expected H_2, H_2O, and O_2 molar flow rates are $Q_{m,H2}=Q_{m,H2O}=2Q_{m,O2}\approx 0.5$mmol/s (~40 stdl/h). The expected reversible ceria reduction extent is $\Delta\delta\approx 0.017$, giving a CeO_2 flow rate $Q_{m,CeO2}\approx 32$mmol/s or Q_{CeO2}~5.5g/s—values relevant to the design of the prototype reactor elements.

A conceptual drawing of the cascading pressure reactor is shown in FIGURE 2a, showing only the salient elements: Two TR chambers (TR1 and TR2), a WS chamber, a particle return elevator, and radiant sources, intended to be a solar simulator. In operation, the reactive oxide particles are heated to the reduction temperature and then reduced in the TR chambers. They then flow (by gravity) to the WS chamber, where they are exposed to steam and reoxidized, producing H_2. Finally, they are returned to the beginning of the cycle by a particle elevator. Pressure separation between various reactor elements is accomplished by the packed beds of small oxide particles. An annotated block-diagram of the reactor prototype is shown in FIGURE 2b.

The roles of the TR and WS chambers and particle elevator are self-explanatory and detailed in previous work.[7, 8] The prototype also requires elements not expected in a full-scale reactor, i.e. "buffer" chambers. These small chambers enable the removal of gasses at intermediate pressures and volumes between the main reactor components. Some of the component design pressures are identical ($p_4=p_7$, and $p_1=p_3$), in order to share vacuum pumps. Chambers with identical gas components are intended to be pumped via common output lines, to minimize the number of pumps, and to enable the accurate evaluation of output gasses ratios, especially H_2/O_2.

Some technical challenges, such as heat losses in a comparatively small device, and the use of high temperature materials, are common in this application space. Others, such as particle conveyance and pressure separation, and gas flow through packed oxide beds, are specific to the design and are described in more detail.

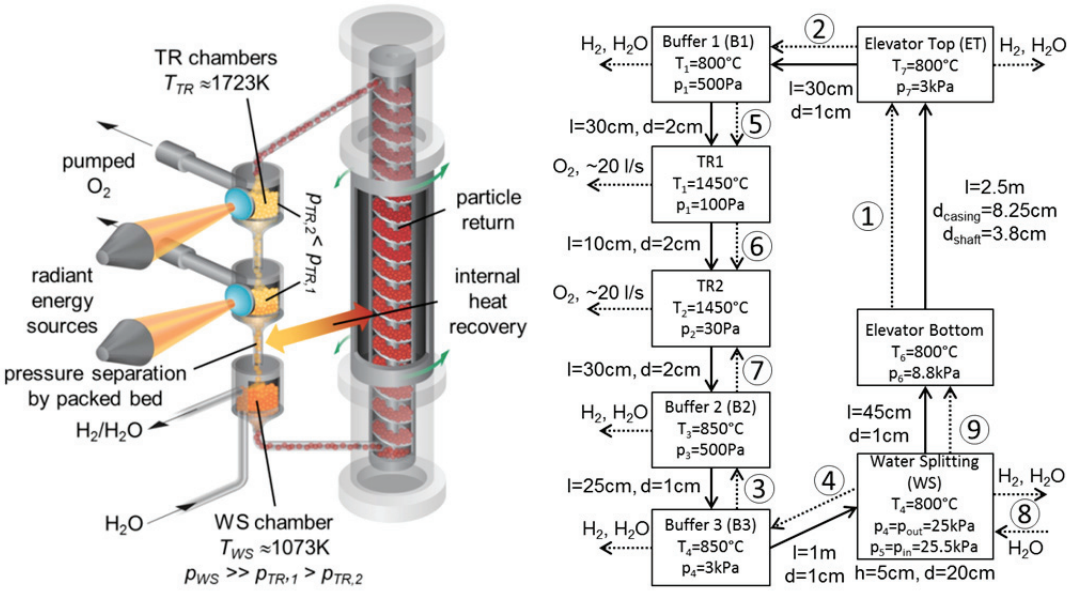

FIGURE 2. (a) Conceptual drawing of the cascading pressure reactor. In the prototype, though not necessarily in a full-size reactor, the particle return is a vacuum Olds Elevator™, with a stationary auger and a cylindrical rotating casing around it, moving particles as a full-bore packed bed.[7, 11] The oxide and steam in the WS chamber flow is countercurrent—a critical design feature, included in the efficiency calculations. (b) Prototype diagram, with loose resemblance to reactor geometry. Solid arrows indicate particle flow, dashed ones gas flows (1-9). Dimensions are of the internal packed particle beds, not the exterior chambers and connecting elements. For brevity, p_{WS} is used in the text when the pressure drop in the WS chamber (p_5–p_4) is irrelevant.

Gas Flows and Pressure Separation Design

The relatively compact size of the prototype (total height <4m, WS—B3 column height <1m) has two consequences: First, a sub-atmospheric p_{WS}, unlike that expected in a full-size reactor. Second, gas expansion from high to low pressure and resulting superficial flow velocity must be carefully considered to ensure that particle beds remain packed. Gas expansion has another consequence—a large volumetric pumping requirement.

Gas volumetric flows (Q) were calculated using a simple Darcy equation for compressible fluids:[12]

$$Q_{p_h-p_l,p_r} = \frac{KA(p_h^2 - p_l^2)}{2\mu L p_r} \quad (1).$$

Here, A is the flow cross-section area, p_h and p_l are the high and low pressures, L is the flow length, and μ is the dynamic viscosity. The reference pressure is p_r=p_l, because the relevant quantity is the flow at the low pressure side. Finally, K is the bed permeability, a function of particle size, approximated by the Rumpf-Gupte model[13]:

$$K = \frac{\varepsilon^{5.5} d^2}{5.6} \quad (2).$$

Here, d is the spherical particle diameter and the void fraction is ε=0.4, appropriate for loose to poured random-packed spheres. All of the results are nearly identical using the Carman-Kozeny permeability model.

The main purpose of the gas flow design is to meet requirements with large margins, owing to uncertainties regarding bed permeabilities. Gas flows between chambers, and especially into TR1 and TR2, must be negligibly small (<1%) compared O_2 pumping speeds (S_{TR}≈20 l/s). A large available flow is required through the WS chamber bed, sufficient to accommodate $Q_{m,H2O}$≈0.5mmol/s. Fluidization must not occur in any of the beds, a requirement especially important in the higher pressure sections (i.e. where gas flow is mostly viscous), but not in the lower pressure sections (where flow is closer to molecular), since fluidization cannot occur in molecular flow.

Entrained gas flow in the bed voids is neglected, being much smaller than S_{TR}: At a solid density ρ_{CeO2}=7.2kg/l, and ε~0.4, the bulk density is $\rho_{CeO2,bulk}$≈4.3kg/l. At Q_{CeO2}≈5.5g/s, the volumetric flow is $Q_{V,CeO2}$≈1.3x10^{-3}l/s, and the void flow $Q_{V,void}$≈5x10^{-4}l/s<<S_{TR}≈20 l/s. Molecular flow effects were neglected for simplicity, and because they are significant only where absolute pressure differences and resulting flows are the lowest, e.g. between TR1 and TR2.

Calculated gas flows rates and velocities, shown in FIGURE 3, are the outcome of a lengthy exploration of the physical dimensions of various bed sections and acceptable TR and WS pressures (noted in FIGURE 2b). The values in FIGURE 3a, should be viewed in light of the design purpose—lower is better (i.e. less cross-flow between chambers), except inside the WS chamber, where a flow higher than the minimum requirement is desirable. To lower flow velocities and avoid bed/column fluidization, cross-section expansions are anticipated (FIGURE 3b).

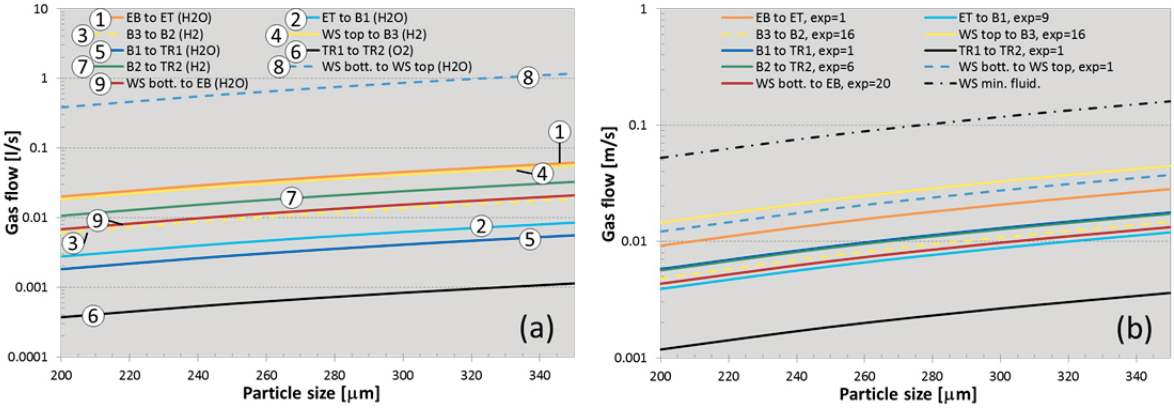

FIGURE 3. (a) Calculated gas flows in the reactor, with gas species indicated in parenthesis. Where more than one species is present, the dominant or limiting one was considered (e.g. the steam flow limit in the WS chamber is lower than that of H_2). (b) Calculated superficial flow velocities the reactor (same legend as in a), with flow cross-section expansion values. As a reference, the minimum fluidization velocity for steam in the WS chamber is also shown. Satisfactory particle flow has been measured for d=200-500μm particles, and pressure separation is robust to at least a d=100-500μm range.

Overall, the results in FIGURE 3a show that gas cross-flows can be negligible, while allowing for a sufficiently high steam flow in the WS chamber (at least ~0.3 l/s at the design pressure). For example, in the WS→B3→B2→TR2 section—all three flows (3, 4, and 7 in FIGURE 3a) are exceptionally low. Without buffer chambers, the WS→TR2 flow would be ~15 l/s (of mostly H_2)—comparable with the TR2 O_2 pumping speed, and nearly sufficient to fully recombine with the TR2 O_2 product. The calculated Q_5, Q_6, and Q_7 values are well below $0.01S_{TR}$, leaving ample margins for contingencies, such as inaccuracies of the simple Darcy model at low pressure.

Gas flow velocities can be reduced to values below fluidization (FIGURE 3b), with considerable margin, by expanding the flow cross-sections at the low pressure sides. Expansion was assumed to be a stepwise tube diameter widening, and short wider tube sections were assumed not to affect the flow rate substantially. The required (or helpful) expansion varies from none in sections (1), (5), (6), and (8) in FIGURE 3, to a maximum of 20, corresponding to a flow diameter increase by less than fivefold (e.g. from 1cm to 5cm). Because fluidization cannot be achieved in molecular flow in the lowest pressure reactor sections, some flow velocities are inconsequential.

The steam flow velocity in the WS chamber (FIGURE 3b) is critical —the bed is wide and it would be difficult to increase its diameter without using a very large chamber. This is also the reason the minimum fluidization velocity (v_f) for steam in the WS chamber is given as a reference (and a worst-case value) in FIGURE 3b. Also critical, but much more manageable is the WS→B3 flow velocity, because a larger flow expansion can be accomplished with relative ease, and because the relevant v_f is that of H_2, substantially higher than for H_2O.

Because the K dependence on d and especially ε, are steep power expressions (Eq. 2), small input changes (e.g attrition-caused) can result in large K changes. It therefore seems prudent to retain design robustness and not eliminate some buffer chambers, despite the low gas cross-flow. Flow rates in FIGURE 3b are unequal, but adjusting segment lengths to achieve identical flows and a minimum sum was not geometrically possible.

Particle Elevator

Design

The particle elevator, shown in FIGURE 4a, is presently the most developed and well-characterized component, serving two purposes: moving reactive particles from the WS chamber, to the cycle beginning in the TR chambers, and pressure separation, by packed bed elevation. The elevator is also a component development test stand,

consisting of three main segments: top and bottom stationary chambers, and a middle rotating segment (MRS). The bottom chamber will receive the reoxidized particles flowing down from the WS chamber (FIGURE 2a). The top chamber will receive the elevator particle discharge and direct it into the TR1 chamber (via B1). The MRS transfers motion to the cylindrical rotating casing (FIGURE 2a), is connected to the stationary chambers via rotating vacuum seals, and is driven by an electric motor with a high gear reduction ratio. The target MRS angular velocity is ω<2rpm. Chambers and connecting elements are standard vacuum components (304 stainless steel), rated to 450°C, using oxygen-free high thermal conductivity (OFHC) copper seals to maintain vacuum (<10^{-11}Pa). While not necessary in a full-size plant, these components are an off-the-shelf solution of great value in the prototype phase.

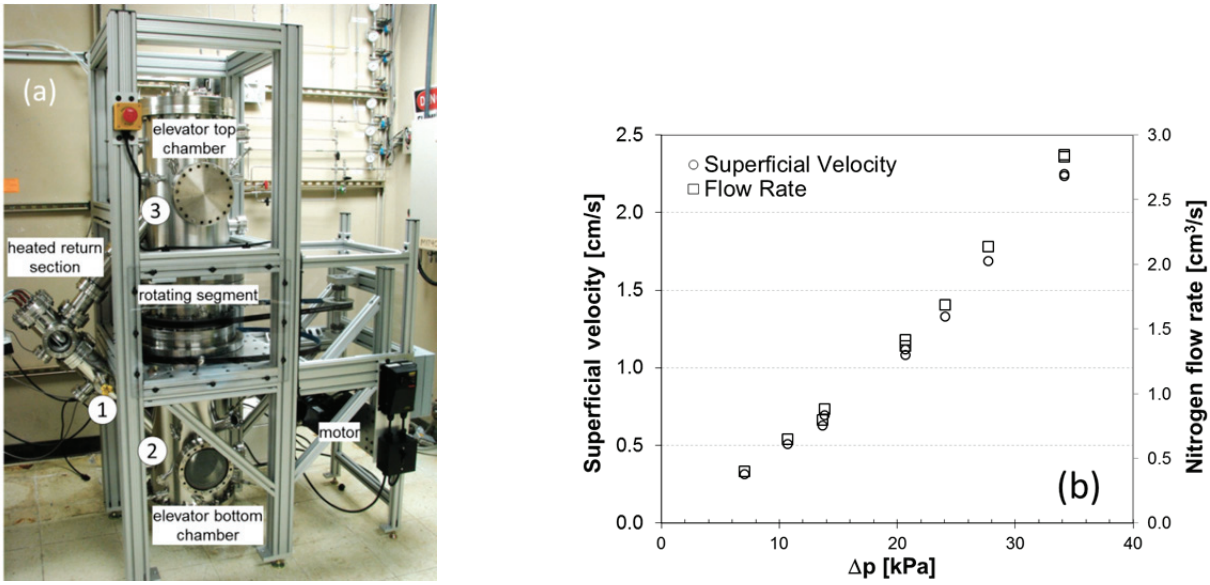

FIGURE 4. (a) Particle elevator/test stand, with main components labeled. (1), (2) and (3) indicate the approximate positions of thermocouples used to measure particle temperature. (1) is in direct contact with the particles, inside the heated section; (2) is on the outside of the outlet tube of the same section (not in direct contact), and (3) is at the top of the return section (also no contact). (b) Measurements of nitrogen flow through a tube packed with steel grit.

To accommodate a substantial amount of high-temperature thermal insulation, the MRS diameter is ~30cm, much larger than the ~9cm OD of the internal rotating casing. The elevator and other components are also intended to be insulated externally (i.e. outside of the vacuum envelope), partly to avoid using overly large (also heavy and expensive) components, but also to keep the interior temperature at >100°C and minimize steam condensation.

Interior 304 stainless steel elements limit T_{WS} to <800°C, which does not maximize efficiency (FIGURE 1), but was judged a good compromise to avoid using costly high-temperature alloys and ceramics. Furthermore, advanced oxides are expected be most efficient at a much lower T_{WS} than ceria, making a high T_{WS} design unwarranted.[9]

Testing

Static and dynamic pressure separation Before designing the elevator, pressure separation by a packed bed was evaluated in a series of tests using, among other materials, steel grit (~180μm particle size, solid density ρ_{steel}≈7.85kg/l, measured bulk density $\rho_{steel,bulk}$~3.6kg/l, giving a ~0.46 void fraction). The particle size and material were chosen to represent ceria (ρ_{CeO2}=7.2kg/l). Nitrogen was introduced at an elevated pressure and ambient temperature at the bottom of a 12.7mm diameter grit-filled vertical tube (h=2.16m), and the flow rate measured at the outlet (at ambient pressure, ~84.3kPa in Albuquerque, New Mexico). Sample results are shown in FIGURE 4b.

Based on the measured gas flow rates, an approximate value for the bed permeability K=2.3x$10^{-11}$$m^2$ was calculated (Eq. 2), in agreement with the Rumpf-Gupte model (K_{RG}=3.96x$10^{-11}$$m^2$) and the Carman-Kozeny model (K_{CK}=2.94x$10^{-11}$$m^2$), when a sphericity factor of 0.7 is accounted for, to give a 126μm effective particle diameter.

The earliest onset of bed fluidization near the outlet was observed at Δp≈79kPa (without affecting pressure separation) and also in line with the theoretical prediction (76.3kPa), based on balancing the gas pressure and bed

weight ($\Delta p_{max}=\rho_{bulk}gh$). These results confirm that flow through a packed unconsolidated bed is severely impeded, is in line with models, and that the concept of the particle bed "seal" is sound.

Dynamic pressure separation tests were conducted in the particle elevator, using spherical bauxite proppants, d≈400μm, nominal solid density $\rho_{proppant}$=3.27kg/l, or about ~2.2 times lower than that of ceria, and a bulk density $\rho_{proppant,bulk}$=1.88kg/l. Beds of spherical particles have higher permeabilities than those of irregular particles of the same size, a disadvantage in this application. Nonetheless, attrition is expected to shape initial geometries into spheres, so consistent results can be achieved using spherical particles from the start. Presently, the elevator particle column is 1.2m tall. The column height relevant to pressure separation is ~48cm, in the lower portion of the heated section (FIGURE 4a), and the maximum Δp for the proppant is 8.85kPa. Dynamic pressure separation tests were conducted at a conservative Δp=4.9kPa (at 100kPa in the bottom chamber), at an angular velocity ω=4rpm (higher than expected in operation), and were completely successful—a dynamic Δp was easily maintained.

Based on an anticipated ceria column height of ~70-80cm between the WS and B3 chambers (FIGURE 2b), the maximum Δp in the full-height prototype is >30kPa—considerably more than the 22kPa design value. Combined with an adjustable p_{WS}, the required Δp should be achieved comfortably by a ceria column.

Particle conveying rate and power requirements The particle elevator was characterized to ensure that a sufficient conveying rate can be achieved in vacuum, at a power substantially lower than the total reactor power input. The results of these measurements are shown in FIGURE 5.

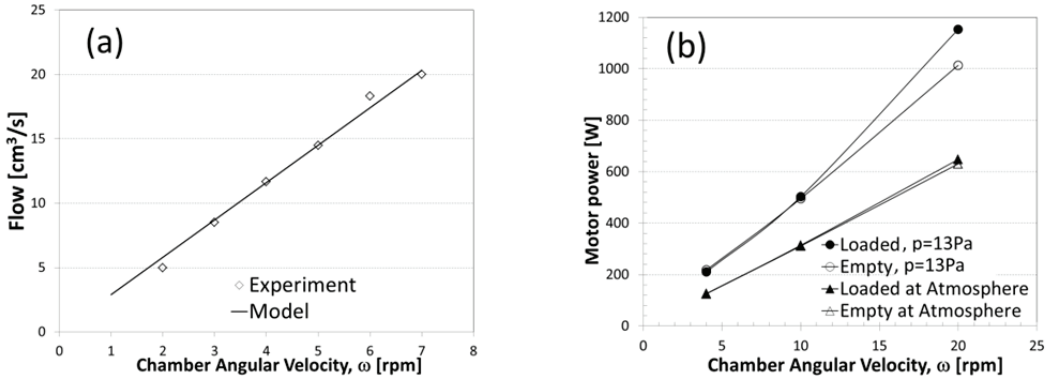

FIGURE 5. (a) Particle conveying rate as function of ω and a model for a conveying efficiency of 0.38. Flow measurements were conducted under ambient conditions. (b) Motor power as function of ω, for several operating conditions (particle load, vacuum).

The theoretical volumetric conveying capacity per revolution is:

$$V = \frac{\pi}{4}(d_{casing}^2 - d_{shaft}^2)P \qquad (3).$$

Here, d_{casing} is the inside diameter of the casing (8.25cm), d_{shaft} is the auger shaft diameter (1.59cm), and P is the auger pitch (8.89cm). The conveying efficiency is the measured conveying rate and theoretical capacity ratio, found to be η_c≈0.38. To achieve the required Q_{CeO2}=5.5g/s ($\rho_{CeO2,bulk}$≈4.3kg/l), the elevator can be operated at 0.4rpm, well below maximum prior experimental velocities. Under consideration is also reducing the casing diameter (to decrease heat losses), and increasing the shaft diameter (to add strength).

To determine the elevator power requirements, measurements were made for a range of ω (FIGURE 5b), with somewhat unexpected results. At low ω, the motor power is identical for the empty and loaded elevator, and small differences become apparent only at high ω. Furthermore, substantially more power is required to rotate the elevator under vacuum, whether empty or full. These results indicate that power is mainly used to overcome parasitic loads (e.g. friction in the seals and transmission elements), and that the elevator power is unlikely to change substantially with ceria, at twice the height (~2.4m), ~5kPa, and ω=1.2rpm, and can be expected to be below 200W.

High temperature tests To validate the elevator conveying capability at high temperature and under vacuum, a series of experiments were conducted at increasingly higher temperatures and lower pressures, with resistive heating in the return section. Results from one continuous experiment are shown in FIGURE 6.

All heated experiments to date have been conducted in an uninsulated elevator, leading to high heat losses and a substantial temperature drop between the heated section and elevator top. Nonetheless, temperatures exceeding

600°C were reached in the heated section. Prolonged heated experiments have also helped identify design weaknesses in the interior components, most notably as they pertain to sensitivity to fouling by fine particles, and the need for higher than customary safety factors for critical mechanical components. Importantly, pumping down and maintaining vacuum at 300°C presented no difficulties, even in the absence of any mitigation techniques, such as cooling gasses before the pump inlet. This finding is encouraging for the TR and WS chambers, discussed below.

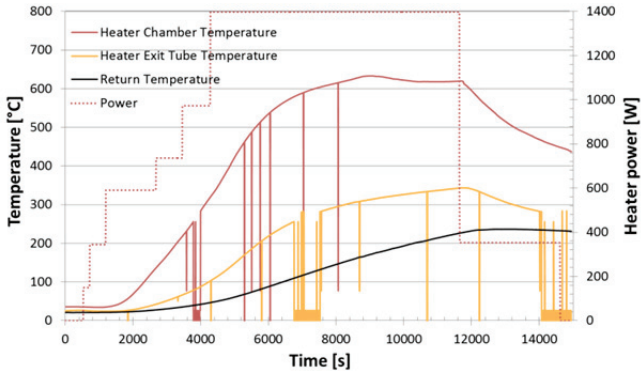

FIGURE 6. High-temperature vacuum operation of the particle elevator. The total duration of the above test was ~6h, of which approximately the first 2/3 are shown in the plot. The remainder consisted of a gradual system cooling. Following an initial pump-down, the pressure in both chambers, throughout the experiment, was ~25Pa. Temperature data was logged by a computer, and "spikes" indicate an intermittent data loss. The difference between the heater chamber temperature—(1) in FIGURE 4a—and the heater exit tube temperature—(2) in FIGURE 4a—may be overstated, because only the former is in direct particle contact.

Thermal Reduction Chambers and the Water Splitting Chamber

Thermal reduction chambers The purpose of the TR chambers is to enable the efficient transfer of the incoming flux to the oxide particles, their heating to T_{TR} and subsequent reduction, and the effective removal of the evolved oxygen. Heating to T_{TR} would be accomplished in TR1, but would be of minor importance in TR2.

One of the challenges in designing the TR chambers is quick and effective heat transfer to the oxide particles. A falling particle approach is not feasible in the prototype—the freefall residence time would be only ~0.2s. The particles must therefore be exposed to radiation as a slowly moving bed, a difficulty because of the low thermal conductivity of particle beds in vacuum.[14] Preliminary experiments and models show that the bed depth and particle dimensions must be comparable to achieve the required heat transfer rate. Mixing options are also being assessed. The section of the bed undergoing reduction, must also be thin enough for unimpeded oxygen flow—opposite of the effect use for pressure separation. Finally, an important consideration is flexibility, e.g. the ability to adjust residence time, whether to tune performance with ceria, to adjust the reduction temperature, or to accommodate other oxides.

To satisfy the above requirements, a thin layer of oxide will be moved through the irradiation zone on a horizontal ceramic plate. The plate will be actuated in a longitudinal reciprocating pattern, causing the particles to move forward in a stick-slip fashion, at a rate that can be controlled by the differential forward and backward acceleration of the plate. Because of the horizontal particle flow, the prototype will use a beam-down solar simulator, in contrast to the conceptual depiction in FIGURE 2a.

The TR chambers will be apertured receivers, with domed quartz windows as vacuum barriers. Pumping O_2 from the TR chambers is challenging, though for somewhat counterintuitive reasons. The mass flow rate Q_{O2}=8mg/s, is of no concern in terms of power or stress/load on pump elements. The heat carried away by the O_2 is also negligible—at $c_{p,O2}\approx$30J/mol K, and $\Delta T_{O2}\approx$1400°C, the heat flux is only $Q_{h,O2}\approx$10W. Vacuum itself is not a difficulty either—most rotary vane or scroll roughing pumps, can reach ultimate pressures of 0.1-1Pa, and have rather flat pumping speed characteristics down to ~10Pa. In this sense, off-the-shelf vacuum pumps are overdesigned for the task.

The main challenge in pumping oxygen from the TR chambers stems from the large volumetric flow at low pressure and high temperature (V~T/p). Off-the-shelf roughing pumps that are most (but not ideally) suited for the target pressure range, are positive displacement pumps with low volumetric pumping speeds. Even with the reduction in required pumping speed achieved by the cascading pressure design, the pumping speeds of existing physically small pumps fall well outside of that ideal for the application. Axial flow pumps would be perfect for the task, by providing a high inlet flow rate and a modest initial compression, e.g. by a factor of 10. After initial

compression, the volumetric flow would be easily handled by higher compression, lower flow pumps, e.g. of the positive displacement or centrifugal type. Unfortunately, no suitably sized axial flow pumps are readily available. The design pumping speeds shown in FIGURE 2b are the result of compromises with the above considerations in mind, and will be achieved using positive displacement pumps.

Water splitting chamber The WS chamber serves to expose the reduced oxide to steam, in a countercurrent flow arrangement, to maximize reoxidation and H_2 production, while minimizing steam input. The main design challenge for the WS chamber is ensuring sufficient steam flow through the bed (~0.3 l/s), without fluidization. This is a *critical design feature* of the reactor, as the H_2O/H_2 ratio is much higher in mixed flow than in countercurrent flow[7, 15], making it essentially impossible to achieve high efficiencies in a mixed flow regime. This requirement is the reason behind the wide, shallow bed dimensions shown in FIGURE 2b.

In the TR chamber buoyancy and drag calculations predict weight/lift<1 for particles larger than ~10μm. In the WS chamber, the same is true for particles larger than ~3μm. Therefore, we anticipate few particles being lifted or carried away by the gasses in any of the chambers.

SUMMARY AND OUTLOOK

To demonstrate continuous H_2 production in a particle based reactor, with all key components (receiver-reactors, water splitting, particle lift, pressure separation) at realistic process temperatures and pressures, we have undertaken a cascading pressure prototype reactor design. Main results of this work to date include: An efficiency model, predicting a prototype efficiency of ~5%; A gas flow and pressure separation analysis, showing that the packed bed approach can be implemented at the relatively small scale; Static pressure separation validation; Particle conveying in vacuum at elevated temperature and with dynamic pressure separation, in a particle elevator that will become a part of the prototype; And a preliminary analysis of design options for the TR chambers and the WS chamber.

Ongoing work is focused on upgrading the particle elevator to improve resiliency to fouling by fines and to increase its operating temperature to at least 800°C. Detailed modeling and experiments are also under way to validate design solutions for the thermal reduction, water splitting and intermediate chambers, as well as the solar simulator and other ancillary components.

ACKNOWLEDGEMENTS

This work is part of a project titled “High Efficiency Solar Thermochemical Reactor for Hydrogen Production”, supported by the U.S. Department of Energy Fuel Cell Technologies Office. Sandia is a multiprogram laboratory operated by Sandia Corporation, a Lockheed Martin Company, for the United States Department of Energy’s National Nuclear Security Administration under Contract DE-AC04-94AL85000.

REFERENCES

1. T. Nakamura, Sol. Energy **19**, 467-475 (1977).
2. E. A. Fletcher and R. L. Moen, Science **197**, 1050-1056 (1977).
3. Y. Tamaura, A. Steinfeld, P. Kuhn, and K. Ehrensberger, Energy **20**, 325-330 (1995).
4. N. Gokon, S. Takahashi, H. Yamamoto, and T. Kodama, Int. J. Hydrogen Energy **33**, 2189-2199 (2008).
5. R. B. Diver, J. E. Miller, M. D. Allendorf, N. P. Siegel, and R. E. Hogan, J. Sol. Energy Eng. **130**, 041001-041001 -041001-041008 (2008).
6. J. Lapp, J. H. Davidson, and W. Lipinski, Energy **37**, 591-600 (2012).
7. I. Ermanoski, N. P. Siegel, and E. B. Stechel, J. Sol. Energy Eng. **135**, 031002-031001 - 031010 (2013).
8. I. Ermanoski, Int. J. Hydrogen Energy **39**, 13114-13117 (2014).
9. I. Ermanoski, J. E. Miller, and M. D. Allendorf, PCCP **16**, 8418-8427 (2014).
10. I. Ermanoski, Energy Procedia **69**, 1731-1740 (2015).
11. http://www.oldselevator.com/, Accessed on 18.Nov.2011
12. H. Darcy, *Les Fontaines Publiques de la Ville de Dijon*, Paris, 1856.
13. H. C. H. Rumpf and A. R. Gupte, Chemie Ingenieur Technik **43**, 367-375 (1971).
14. M. Shapiro, V. Dudko, V. Royzen, Y. Krichevets, S. Lekhtmakher, V. Grozubinsky, M. Shapira, and M. Brill, Part. Part. Syst. Charact. **21**, 268-275 (2004).
15. P. T. Krenzke and J. H. Davidson, Energy Fuels **29**, 1045-1054 (2015).